Extent of cortical generators visible on the scalp: effect of a subdural grid

Nicolás von Ellenrieder[ab1*], Leandro Beltrachini[c1], Carlos H. Muravchik[b], and Jean Gotman[a]

[a] Montreal Neurological Institute and Hospital
3801 University Street, Montreal, Quebec, H3A 2B4, Canada

[b] LEICI, Facultad de Ingeniería, Universidad Nacional de La Plata
Calle 1 y 47, La Plata, Buenos Aires, B1900TAG, Argentina.

[c] CISTIB, The University of Sheffield
Sir Frederick Mappin Bldg, Mappin Street, S1 3JD Sheffield, UK

* Corresponding author:
Montreal Neurological Institute
3801 University Street, Room 009d
Montreal, QC H3A 2B4, Canada
nellen@ieee.org
phone: +1 514 398 6644, ext 00445
fax: +1 514 398 8106

[1] Both authors contributed equally.

Highlights

- Subdural grids attenuate the scalp potential of generators located under them.
- Attenuation of subdural grids and amplification of skull holes do not cancel each other.
- Minimum cortical extents of visible scalp activity could be smaller than previously reported.

Abstract

The effect of the non-conducting substrate of a subdural grid on the scalp electric potential distribution is studied through simulations. Using a detailed head model and the Finite Element Method we show that the governing physics equations predict an important attenuation in the scalp potential for generators located under the grid, and an amplification for generators located under holes in the skull filled with conductive media. These effects are spatially localized and do not cancel each other. A 4 x 8 cm grid can produce attenuations of 2 to 3 times, and an 8 x 8 cm grid attenuation of up to 8 times. As a consequence, when there is no subdural grid, generators of 4 to 8 cm^2 produce scalp potentials of the same maximum amplitude as generators of 10 to 20 cm^2 under the center of a subdural grid. This means that the minimum cortical extents necessary to produce visible scalp activity determined from simultaneous scalp and subdural recordings can be overestimations.

Keywords

Electrocorticography, subdural grid, scalp EEG, Finite Element Method.

1. Introduction

Early studies of the extent of cortical generators producing visible scalp activity from the brain hinted at minimum extents of around 6 cm^2 (Cooper et al., 1965; Kobayashi et al., 2005; Cosandier-Rimélé et al., 2008). This value should be taken only as an approximation, since the experimental work was an in vitro measurement involving only the skull (Cooper et al., 1965), and the values obtained from simulation studies (Kobayashi et al., 2005; Cosandier-Rimélé et al., 2008) are highly dependent on uncertain parameters such as the skull conductivity and the generator strength per unit area.

Later, simultaneous recordings of scalp EEG and intracranial EEG with a subdural grid were performed, and 10 to 20 cm^2 of cortex was found to be the minimum extent necessary to generate ictal and interictal

epileptic discharges (Tao et al., 2005; 2007a; 2007b; Hashiguchi et al., 2007) detectable in the scalp in clinical frequency ranges (0.1 - 40Hz). Therefore, a 10 to 20 cm^2 extent limit is the currently accepted value in the EEG community. However, the results from these simultaneous scalp and subdural EEG studies rely on the untested assumption that the presence of the subdural grid does not affect the electric potential distribution on the scalp, or that the effect of the non-conducting substrate of the grid is canceled out by the effect of holes in the skull due to the grid implantation craniotomy (Tao et al., 2007a).

In this work we report the results of detailed and exhaustive simulations studying the effect of the subdural grid and skull holes in the scalp electric potential distribution. We compare the scalp potential with subdural grids of different sizes, subdural grids in and skull holes, and subdural grids with holes in the non-conducting substrate (fenestrated grids), to the scalp potential when no grid is present. Such a fenestrated grid was proposed by Tao et al. (2007a) as a possible solution to minimize the effect of the grid on the scalp potential.

2. Methods

We solved the Maxwell equations in a realistic head model using the Finite Element Method (FEM). A detailed head model was built based on the Colin27 high resolution MRI segmentation of the Montreal Neurological Institute (Aubert-Broche et al., 2006). A mesh with more than 8 million tetrahedral elements was created using the iso2mesh software (Fang and Boas, 2009). This resulted in tetrahedra of less than 1 mm side, with local refining in the neighborhood of the cortex. Isotropic conductivity was assumed for the 8 tissues included in the model: skin and muscle (0.435 S/m), fat (0.078 S/m), bone (0.0064 S/m), marrow (0.0286 S/m), major blood vessels (0.49 S/m), cerebrospinal fluid (CSF; 1.79 S/m), gray matter (0.333 S/m), and white matter (0.142 S/m). The electric conductivity values were selected from the relevant literature (Bauman et al., 1997; Ramon et al., 2006; Gabriel et al., 2009; Dannhauer et al., 2011; Choi et al., 2012). A slice of the head model showing the mesh and electric conductivity is shown in Fig. 1a. We adopted a geometrically detailed model including many different tissues and isotropic conductivity instead of a coarser model with anisotropic conductivity and the same computational load because, for scalp recordings, an accurate model of the CSF is more important than white matter anisotropy (Wolters et al., 2006), and for the skull, modeling the distinction between hard bone and marrow is more important than modeling skull anisotropy (Dannhauer et al., 2011).

To model the generators of epileptic activity, we built a cortical surface as the mid-surface between the CSF - gray matter interface and the gray matter – white matter interface using the Freesurfer software

(Dale et al., 1999). The total cortical surface of the left hemisphere was tessellated in more than 330,000 triangular elements. We simulated generators centered in each vertex of the left frontal lobe tessellation, in approximately 58,000 different locations. In each location, generators with different spatial extents were modeled. Each of these distributed generators was modeled as a set of dipoles on the vertices of the cortical surface, with orientation normal to the surface, and a smooth intensity profile weighted by the area of the surrounding triangles (von Ellenrieder et al., 2009). Since the support of the generators was defined using the geodesic distance to the center of the generator, its actual area depends on the curvature of the involved portion of the cortical surface. In experimental studies the extent of a generator is often computed based on the number of channels showing activity on a subdural grid (Tao et al., 2005; 2007a; 2007b; Hashiguchi et al., 2007). For comparison purposes we report the extent of the generators as the area of the projection of the generator onto the inside of the skull. To compute this subdural extent we projected the cortical generator on the surface delimiting the inside of the skull, in the direction given by the segment joining the center of the generator and the nearest point on the skull. The subdural extent is then always lower than the actual geodesic extent on the cortical surface, especially for generators on sulcal walls. An example of a generator and its projection on the skull inner surface can be seen in Fig. 1f.

We modified the original head model to obtain other models including subdural grids, and some models including also holes in the skull. The non-conducting substrates of 8 x 8 cm and 4 x 8 cm subdural grids, as well as a 1 x 8 cm subdural strip, were included in the models over the left frontal lobe. The grids substrate of 1.5 mm thickness was modeled under the skull, leaving a 1.5 mm gap between the skull and the grids which was assumed to be filled by CSF. A smooth linear deformation was applied to the limit surfaces between CSF and gray matter, and between gray and white matter, to avoid contact between these surfaces and the subdural grid. The deformation extended to a depth of 7.5 mm under the skull, and was hardly noticeable on the cortical surface (see Fig. 1b). Four holes with 10 mm diameter were included in some models. The holes were located close to the corners of the grids, with a homogeneous filling of high conductivity (1 S/m). Skull holes are usually filled by CSF, blood, cable bundles, and air bubbles, and we believe the bulk conductivity is probably lower, but chose a high value to account for the worst case, i.e. the effect of the holes will probably be less noticeable in real measurements than in this simulation. We also modeled two fenestrated 8 x 8 cm grids, with round holes in the substrate in the spaces between contacts. In one of the models the holes had a diameter of 6 mm and 10 mm spacing in each direction, and in the other the holes had 1 mm diameter and 1/3 cm spacing (except in the grid contacts). In both cases the total area of the holes was approximately ¼ of the 64 cm^2 of the original grid. The subdural grid and skull holes models can be seen in Fig. 1.

We adopted the usual quasistatic approximation of Maxwell equations (Geselowitz, 1967). This approximation is valid in the head tissues for frequencies up to several kHz (Hämäläinen et al., 1993). The conductivity inside the subdural grid is zero, with neither ionic nor electronic conduction. There are displacement currents inside the dielectric substrate of the grid, but the effect of these displacement currents is negligible in the electric potential distribution outside the grid, as discussed in the accompanying Supplementary File S1. The computation of the electric potential distribution was done with a Galerkin formulation of the FEM, assuming linear variation of the electric potential on each element (Hutton, 2004; Wolters et al., 2006).

We computed the electric potential on 329 points on the scalp corresponding to the locations of the 10-5 electrode placement system (Oostenveld and Praamstra, 2001; Jurcak et al., 2007). In the figures showing the scalp electric potential distribution the values were linearly interpolated to other points on the scalp for aesthetic reasons only.

The detectability of a signal on the scalp depends not only on the amplitude of the electric potential produced by the cortical generator, but also on the noise level. The main contribution to the noise is from background brain activity unrelated to the generator under study (Horikawa et al., 2003). This background activity can be modeled as a set of random dipoles on the cortex (de Munck, 1992). For each head model, we computed the standard deviation of the scalp potential of 6000 dipolar generators randomly distributed on both hemispheres of the cortical surface. This model may not be totally adequate for breach artifacts, which would be modeled as generators located very close to the holes, and not as background activity. We computed the ratio of the scalp potential standard deviations of the models with and without the subdural grid to quantify the effect of the subdural grids and skull holes on the scalp noise level.

3. Results

First, we studied the effect of the grid on generators located close to the position of the 4 x 8 cm subdural grid, modeling the generators of epileptic ictal or interictal activity. Figure 2 shows the amplification/attenuation factor of the maximum absolute scalp potential for generators of different extent: dipolar generators and distributed generators of 4 and 10 cm^2 extent. The color of each point on the left frontal lobe cortical surface corresponds to the amplification factor of a generator centered at that point. The amplification factor is the ratio between the maximum absolute electric potential on the scalp between the models with the subdural grid and the model without the subdural grid. A value greater

than one indicates that the presence of the grid or the skull holes leads to a larger value of the peak scalp electric potential. Values below one indicate attenuation. The results are shown in a more compact way in Fig. 2c and 2f, in a scatter plot where each of the 58000 generators on the cortical surface of the left frontal lobe is represented by a point showing the corresponding amplification or attenuation factor and the distance between the center of the generator and the nearest grid border, both projected on the subdural surface. A larger variability of the amplification factor is observed for smaller generators. This is expected since small generators have more diverse orientation and depth. Generators of large extent have an important overlap when their centers are close, leading to smoother results. For the model with no holes in the skull, amplification factors of up to 2 are seen for small generators precisely under the border of the grid; this amplification can be explained by a local increase of the current towards the scalp near the grid border, given that it cannot flow through the grid. For large generators this effect is not important and the only effect of the grid is the attenuation of generators under it. This attenuation can reach a factor of 3 for 10 cm^2 generators centered under the center of the grid, although attenuation factors around 2 are more common. Smaller generators can have even larger attenuation factors, if centered on the gyri, and less attenuation if located on the sulci. In the model including holes in the skull, amplification factors of up to 8 can be observed for dipolar generators, but decrease for more extended generators. Generators with 10 cm^2 extent show amplification factors of up to 3 when centered under the holes. Note however that the effect is very local, and the attenuation factors for generators under the subdural grid remain essentially unchanged between the models with and without grid holes.

In Fig. 3 we show an example of a generator with extent close to 10cm^2 located under the center of the grid, corresponding to one of the extreme cases with large attenuation (3 times). The figure shows the extent of the source on the cortex, and the electric potential distribution on the scalp for the model without subdural grid and the models with the 4 x 8 grid with and without skull holes. The difference between the models with and without grid is also shown. In all the cases the scalp electric potential difference is localized right over the grid and the skull holes. Hence, not only the effect is observed for generators close to the grid or holes, but also it is noticeable on the scalp only near the grid and holes.

The attenuation produced by subdural grids of different size are presented in Fig. 4. An 8 x 8 grid will attenuate up to 8 times the scalp potential of a 10 cm^2 generator under its center, while the attenuation of a 1 x 8 cm strip is negligible. The effect of fenestrations in the large 8 x 8 cm grid is shown in Fig. 5. The attenuation for 10 cm^2 generators is slightly larger for the grid with small fenestrations than for the one with larger fenestrations, but in both cases the effect seems negligible, especially if compared to the attenuation level of the grid with no fenestrations. In all these models, the effect of skull holes was not

included to facilitate the comparison. The effect of skull holes would be similar in all the cases, and in the case of the subdural strip and fenestrated grids, it would be the dominant effect.

Next, we analyzed how the subdural grids and skull holes affect the scalp potential associated with the background brain activity. We computed the ratio of the background level on the scalp between the models with a subdural grid and the model without the grid. The results are shown in Fig. 6, where a slight attenuation of the background level is observed over the grids, and a slight amplification over the skull holes. The attenuation is around 10% for the 4 x 8 cm grid, 25% for the 8 x 8 cm grid, and negligible for the fenestrated 8 x 8 cm grid. The amplification due to the skull holes is around 25% in all cases. The fenestrated grid does not affect the background activity level on the scalp. It may seem surprising that the background activity is attenuated only 10% over the 4 x 8 cm grid while a generator under the grid is attenuated 3 times. However, due to the spatial smoothing of the scalp potential by the skull, the background activity measured at any point on the scalp is not generated only in the cortex below it, but also in more distant cortical regions. As long as the background brain activity model contemplates simultaneous electric activity in many different cortical regions (de Munck, 1992), the attenuation of the background activity by the subdural grid will be smaller than the worst case attenuation of a single generator.

We also studied how the amplification/attenuation associated with the subdural grid and skull holes may affect the results of joint scalp and subdural measurements. Assuming the electric potential produced by 10 cm^2 generators under a 4 x 8 cm subdural grid is at the limit of detectability on the scalp (Tao et al., 2007a), we looked at the extent of generators that in the absence of the grid produce the same signal to noise ratio on the scalp as a 10cm^2 generator centered at the same point but with a 4 x 8 cm grid. The attenuation of the background activity and the attenuation of the generators are combined to obtain this result. A generator under the grid will produce a smaller electric potential signal on the scalp than if there was no grid, but the background brain activity will also be somewhat lower, making the detection a little less difficult. The results in Fig. 7c show that when there is no subdural grid, a significant proportion of generators between 4 and 5 cm^2 can reach the same signal to noise ratio on the scalp as 10cm^2 generators located under the center of a 4 x 8 cm subdural grid. The situation reverses for generators under skull holes, but the implications are less significant, since the ideal position of the grid is directly above the generators of epileptic activity. An extreme example of the scalp electric potential resulting from a generator of 10.2cm^2 under the grid and one of 2.5 cm^2 centered at the same location in the model without grid is shown in Fig. 8. While this is an extreme case, and such small generators are highly unlikely to produce visible scalp activity, the example shows that in rare occasions it could happen. This indicates

that any limit regarding the extent of cortical involvement necessary for scalp detectability should not be interpreted as a hard limit.

Finally, Fig. 9 shows an example of the electric current distribution inside the head for the models without grid, with grid, and with fenestrated grid. The figure was drawn using the line integral convolution technique (Cabral and Leedom, 1993). The current does not go through the grid, resulting in an important attenuation of the current density and electric potential over the grid. The attenuation is not complete because there is some current flow on the tissues above the grid. The figure also shows how the changes in the current density are restricted to the proximity of the grid. In the model with fenestrated grid the current flows through the grid holes leading to a current distribution almost identical to the no grid case.

4. Discussion

We found important attenuation and amplification for sources close to the subdural grid and skull holes respectively. The effects are quite local, restricted to cortical generators under the grid and holes, and affecting only the scalp potential over them. The amplification due to the skull holes does not cancel out with the attenuation due to the grid. For sources under the center of the grid, the attenuation is important and scalp signals of the same amplitude are produced by generators significantly smaller when there is no subdural grid.

We would like to point out that while this is a simulation study, we are confident that the results are robust and point to a phenomenon that is present in actual measurements. There are several reasons for our confidence in the simulation results. The most important is that they are based on comparison between pairs of models. In this way the effect of the uncertain parameters in usual simulations is greatly reduced. For instance, one of the most important parameters in a scalp electric potential computation is the strength of the generators, i.e. the dipolar moment per unit area of the distributed sources. We do not need to adopt a particular value for this highly uncertain parameter since we only assume that it will be the same in all the models, unaffected by the presence of the grid. The effect of other parameters such as the conductivity of the tissues or the cortical thickness is highly reduced as well in such a study comparing pairs of models. In other words, the best way to study the effect of the subdural grid on the scalp EEG is by comparing the simulation results between models which only differ in the inclusion of the grid. Also, we used an extremely detailed model, with accurate geometric representation of the limits between tissues, and including many tissues. Finally, our results and conclusions are based on scalp electric potentials only. We avoid the simulation of subdural electric potentials since the validity of the

usual models adopted in scalp simulations for the generators, the background activity, and the electrodes has not been tested in detail for subdural recordings.

Our results show a variation of less than 30% in the noise or background activity level, consistent with reports from experimental situations in which the variation seemed unnoticeable (Tao et al., 2007a). The highly localized effect of the subdural grid and skull holes also accounts for this limited background variation. The background activity is generated by the whole brain, and only the relatively small proportion generated near the grid and holes will be affected by them. Then, the overall level of background activity on the scalp will not change very much. The localized effects of the grid and holes also result in poor cancellation of their opposing effects. As a result, if the location of the subdural grid was properly selected to study cortical sources under it, the scalp electric potential of these sources will suffer an important attenuation, regardless of the presence of holes in the skull. The attenuation is not complete in the scalp above the subdural grid because of currents flowing in the higher conductivity paths such as the CSF between the grid and skull, the marrow inside the skull, and the muscle tissue of the scalp.

We found that generators with extents as small as 4 or 5 cm^2 could produce activity in the scalp with the same signal to noise ratio as the 10 cm^2 generators reported to be involved in the production of scalp Interictal Epileptic Discharges (IEDs) when the subdural grid is present. Other values found in the literature, based on experimental or simulation studies are close to the lower end of this range. An often cited experimental study on the size of cortical generators producing detectable scalp activity is the seminal study of Cooper (1965). It is an in-vitro study involving only the skull (no CSF or brain matter), and unipolar generators instead of dipolar layers. The reported 6 cm^2 extent is then necessarily an approximation, and cannot be expected to be very accurate. Experimental evidence could also be gathered from stereo EEG. The depth electrodes used in stereo EEG do not significantly affect the electric potential distribution (von Ellenrieder et al., 2012), but the depth recordings can only provide lower bounds for the extent of the generators, since they provide only a sparse sampling of the cortex. Generators larger than 3 or 4 cm^2 were reported to produce scalp IEDs (Merlet and Gotman, 1999). Simultaneous measurements with dense array scalp EEG and subdural strips also showed some scalp IEDs associated with cortical activity in 2 to 4 contacts, with a mixture of 5 and 10 mm intercontact distance (Yamamoto, 2012).

The relationship between cortical extent of the generators and the amplitude of the related scalp EEG was also studied with simulations (Kobayashi et al., 2005; Cosandier-Rimélé et al., 2008). The drawback of using simulations is that the extent of the cortical generators is almost linearly related to the amplitude

of the resulting electric potential, but it almost does not affect the shape of the scalp electric potential distribution. The same can be said for the skull conductivity, as shown by the isolated skull approach in the integral formulation of the problem (Meijs et al., 1989). And also the generator strength or intensity per unit area affects only the amplitude of the scalp potential (Geselowitz, 1967). Hence, it is almost impossible to distinguish the effect of these three parameters in scalp EEG measurements. As a consequence, to obtain reliable values for the extent of the generators, the simulations must use reliable values for the skull conductivity and generator strength. The values found in recent literature for the skull conductivity range between .0075 and .015 S/m (Oostendorp et al., 2000; Dannhauer et al., 2011), and there is at least a 25% intersubject variability (Dannhauer et al., 2011). The generator strength is an even more uncertain parameter. In some studies it was derived from evoked responses in animal models: rat (Di et al., 1990; Ahrens and Kleinfeld, 2004; Higley and Contreras. 2007), mouse (Mégevand et al., 2008), frog (Nicholson and Freeman, 1975), cat (Pollen, 1969; Freeman, 1975), monkeys (Kraut et al., 1985; Lakatos et al, 2008). The values are inferred from laminar measurements of the electric potential and involve the approximation of second order electric potential derivatives by differences between electrode contacts, a technique highly sensitive to noise. The gray matter conductivity value also affects the results, yielding values for the generator strength between 30 and 250 nA/mm² for volumetric dipolar density, with high variations not only among species but also within species in different brain regions (Ahrens and Kleinfeld, 2004). The resulting values are undoubtedly uncertain, even more so if we consider that they are obtained from evoked responses in animals and assumed to hold for human pathologic generators. Hämäläinen et al. (1993) propose a range from 100 and 250 nA/mm² for the generator strength. Cosandier-Rimélé et al. (2008) selected the lowest values of skull conductivity (.0075 S/m) and generator strength (100 nA/mm²) of the mentioned ranges, and obtained a generator extent of around 7 cm^2 as the detectability limit on the scalp. With higher skull conductivity or generator strength they would have gotten generators of lower extent producing similar scalp signals.

Kobayashi et al. (2005) used the same low skull conductivity and generator strength values and consequently found similar extents (around 6 cm^2) for the generators producing barely distinguishable activity on the scalp. In this case the generator strength was obtained from human sEEG recordings of IEDs, from a different study (Alarcon et al., 1994). However, the value was obtained from spikes by looking at the electric potential difference between two neighboring contacts in the only depth electrode, among 6 patients, in which a typical dipolar pattern was found for the electric potential distribution. The underlying assumption to compute the generator strength in this way is that the extent is large compared

to the separation between contacts, and that was probably not the case since these particular spikes did not generate visible signals in nearby subdural electrodes (Alarcon et al., 1994).

We might conclude that the cortical extent of 6 cm^2 reported by Cooper et al. (1965) is only an indication of the order of magnitude of the cortical generators producing detectable scalp IEDs. Based on simultaneous scalp and subdural EEG recordings not taking into account the effect of the grid, the actual values were believed to be two or three times higher. But they could also easily be somewhat lower as suggested by the results of this work and the choice of parameters in the simulation studies discussed above.

Different approaches could be taken to further study the extent of cortical generators of IEDs. One possibility could be to use simultaneous scalp EEG and MEG measurements. The magnetic field is less affected by the skull than the electric potential, and in consequence not only the amplitude but also the spatial distribution of the field changes for generators of different extent. This could be used for the estimation of the extent of cortical generators which produce visible scalp activity (Chowdhury et al., 2013). Another possibility would be to use detailed head models including the cortical grid to estimate the generators in simultaneous subdural and scalp measurements. However, both of these approaches require the solution of the inverse problem, i.e. the estimation of the generator parameters. This not only involves the need to choose many parameters such as the conductivity of the tissues, but it is also necessary to make prior assumptions regarding the generators to choose one solution among the infinitely many of the inherently ill posed inverse problem. According to our simulation results, the most straightforward way to study the extent of the generators would be the use of fenestrated subdural grids, as proposed by Tao et al. (2007a). Such grids would have a negligible effect on the scalp electric potential distribution. The holes and breaches in the scalp could be covered by a non-conducting material to avoid amplification. However, the use of fenestrated grids could produce cortical injury if the cortical tissue herniates through the holes. Our results show that small fenestrations with 1 mm diameter, much less likely to allow tissue herniation, are as effective as grids with larger fenestrations. Whatever method is chosen to study the issue, no hard limit should be expected on the extent of cortical generators that produce detectable scalp activity. Given the large inter and intra-subject variability in many of the involved parameters (von Ellenrieder et al., 2014), a broad diffuse range should be expected.

In conclusion, our results suggest that the minimum extent of cortical generators of epileptic discharges visible on the scalp is lower than the usually accepted values of 10 to 20 cm^2, with a high probability of generators in the range from 4 to 8 cm^2 producing a visible scalp activity. The difference is explained by

the attenuation of the scalp potential by the non-conducting substrate of the cortical grid in simultaneous scalp and cortical recordings. The significance of these results may extend beyond the study of epilepsy, since many recent neurological studies are based on measures obtained from subdural grids in implanted patients.

Acknowledgements

This work was funded by the Canadian Institute of Health Research (CIHR) grant MCP-38079, Argentina ANPCyT grant PICT 2011-0909, and Universidad Nacional de La Plata grant 11-I-166.

References:

Ahrens KF, Kleinfeld D (1994): Current Flow in Vibrissa Motor Cortex Can Phase-Lock With Exploratory Rhythmic Whisking in Rat. J Neurophysiol 92:1700-1707.

Alarcon G, Guy CN, Binnie CD, Walker SR, Elwes RDC, Polkey CE (1994): Intracerebral propagation of interictal activity in partial epilepsy: implications for source localization. J Neurol Neurosurg Psychiatry 57:435-449

Aubert-Broche B, Evans AC, Collins DL (2006): A new improved version of the realistic digital brain phantom. NeuroImage 32:138–145.

Baumann SB, Wozny DR, Kelly SK, Meno FM (1997): The Electrical Conductivity of Human Cerebrospinal Fluid at Body Temperature. IEEE Trans Biomed Eng 44:20-23.

Cabral B, Leedom L (1993): Imaging vector fields using line integral convolution. In: Proceedings of SIGGRAPH 1993 conference. p 263–272.

Choi HW, Jansen B, Zhang ZD, Kassab, GS (2012): Impact of surrounding tissue on conductance measurement of coronary and peripheral lumen area. J. R. Soc. Interface, published online.

Chowdhury RA, Lina JM, Kobayashi E, Grova C (2013): MEG Source Localization of Spatially Extended Generators of Epileptic Activity: Comparing Entropic and Hierarchical Bayesian Approaches. PLOS ONE 8:e55969.

Cooper R, Winter AL, Crow HJ, Walter WG (1965): Comparison of Subcortical, Cortical and Scalp Activity Using Chronically Indwelling Electrodes in Man. Electroencephalogr Clin Neurophysiol 18:217-228.

Cosandier-Rimélé D, Merlet I, Badier JM, Chauvel P, Wendling F (2008): The neuronal sources of EEG: Modeling of simultaneous scalp and intracerebral recordings in epilepsy. NeuroImage 42:135–146.

Dale AM, Fischl B, Sereno MI (1999): Cortical Surface-Based Analysis I: Segmentation and Surface Reconstruction. NeuroImage 9:179-194.

Dannhauer M, Lanfer B, Wolters CN, Knösche TR (2011): Modeling of the Human Skull in EEG Source Analysis. Human Brain Mapping 32:1383–1399.

de Munck JC, Vijn PCM, Lopes da Silva FH (1992): A random dipole model for spontaneous brain activity. IEEE Trans Biomed Eng 39:791–804.

Di S, Baumgartner C, Barth DS (1990): Laminar analysis of extracellular field potentials in rat vibrissa/barrel cortex. J Neurophysiol 63:832-840.

Fang Q, Boas D (2009): Tetrahedral mesh generation from volumetric binary and gray-scale images. In: Proc. of IEEE International Symposium on Biomedical Imaging. p 1142-1145.

Freeman WJ. 1975. Mass action in the nervous system. Academic Press.

Gabriel C, Peyman A, Grant EH (2009): Electrical conductivity of tissue at frequencies below 1 MHz. Phys Med Biol 54:4863–4878.

Geselowitz DB (1967): On Bioelectric Potentials in an Inhomogeneous Volume Conductor. Biophys J 7:1–11.

Hämäläinen M, Hari R, Ilmoniemi R, Knuutila J, Lounasmaa O (1993): Magnetoencephalography--theory, instrumentation, and applications to noninvasive studies of the working human brain. Rev Mod Phys 65:1-93.

Hashiguchi K, Morioka T, Yoshida F, Miyagi Y, Nagata S, Sakata A, et al. (2006): Correlation between scalp recorded electroencephalographic and electrocorticographic activities during ictal period. Seizure 16:238-247.

Higley MJ, Contreras D (2007): Cellular Mechanisms of suppressive interactions between somatosensory responses in vivo. J Neurophysiol 97:647-658.

Horikawa M, Harada H, Yarita M (2003): Detection Limit in Low-amplitude EEG Measurement. J Clin Neurophysiol 20(1):45–53.

Hutton DV. 2004. Fundamentals of Finite Element Analysis. The McGraw-Hill Companies.

Jurcak V, Tsuzuki D, Dan I (2007): 10/20, 10/10, and 10/5 systems revisited: Their validity as relative head-surface-based positioning systems. Neuroimage 34:1600–1611.

Kobayashi K, Yoshinaga H, Ohtsuka Y, Gotman J (2005): Dipole modeling of epileptic spikes can be accurate or misleading. Epilepsia 46:397-408.

Kraut MA, Arezzo JC, Vaughan HG (1985): Intracortical generators of the flash VEP in monkeys. Electroencephal Clin Neurophysio 62:300-312

Lakatos P, Karmos G, Mehta AD, Ulbert I, Schroeder CE (2008): Entrainment of Neuronal Oscillations as a Mechanism of Attentional Selection. Science 320:110-113.

Mégevand P, Quairiaux C, Lascano AM, Kiss JZ, Michel CM (2008): A mouse model for studying large-scale neuronal networks using EEG mapping techniques. Neuroimage 42:591-602.

Meijs JWH, Weier OW, Peters MJ, van Oosterom A (1989): On the numerical accuracy of the boundary element method. IEEE Trans Biomed Eng 36:1038–1049.

Merlet I, Gotman J (1999): Reliability of dipole models of epileptic spikes. Clin Neurophysiol 110:1013-1028.

Nicholson C, Freeman JA (1975): Theory of Current Source-Density Analysis and Determination of Conductivity Tensor for Anuran Cerebellum. J Neurophysiol 38:356-368.

Oostendorp TF, Delbecke J, Stegeman DF. The conductivity of the human skull: Results of in vivo and in vitro measurements. IEEE Trans Biomed Eng 2000; 47(11):1467–1492.

Oostenveld R, Praamstra P (2001): The five percent electrode system for high-resolution EEG and ERP measurements. Clin Neurophysiol 112:713–719.

Pollen DA (1969): On the generation of neocortical potentials. In Basic mechanisms of the epilepsies. Jasper ed. Oxford University Press.

Ramon C, Schimpf PH, Haueisen J (2006): Influence of head models on EEG simulations and inverse source localizations. BioMed Eng OnLine 2006:5-10.

Tao JX, Ray A, Hawes-Ebersole S, Ebersole JS (2005): Intracranial EEG substrates of scalp EEG interictal spikes. Epilepsia 46:669-676.

Tao JX, Baldwin M, Hawes-Ebersole S, Ebersole JS (2007a): Cortical substrates of scalp EEG epileptiform discharges. J Clin Neurophysiol 24:96–100.

Tao JX, Baldwin M, Ray A, Hawes-Ebersole S, Ebersole JS (2007b): The Impact of Cerebral Source Area and Synchrony on Recording Scalp Electroencephalography Ictal Patterns. Epilepsia 48:2167–2176.

Yamazakia M, Tucker DM, Fujimoto A, Yamazoe T, Okanishi T, Yokota T, Enoki H, Yamamoto T (2012): Comparison of dense array EEG with simultaneous intracranial EEG for interictal spike detection and localization. Epilepsy Res 98:166-173.

von Ellenrieder N, Valdés-Hernández PA, Muravchik CH (2009): On the EEG/MEG forward problem solution for distributed cortical sources. Med Biol Eng Comput 47:1083-1091.

von Ellenrieder N, Beltrachini L, Muravchik CH (2012): Electrode and brain modeling in stereo-EEG. Clin. Neurophysiol 123:1745-1754.

von Ellenrieder N, Beltrachini L, Muravchik C, Gotman J (2014): Size of cortical generators of epileptic interictal events and visibility on scalp EEG. NeuroImage 94:47-54.

Wolters CH, Anwander A, Tricoche X, Weinstein D, Koch MA, MacLeod RS (2006): Influence of tissue conductivity anisotropy on EEG/MEG field and return current computation in a realistic head model: A simulation and visualization study using high-resolution finite element modeling. NeuroImage 30:813-826.

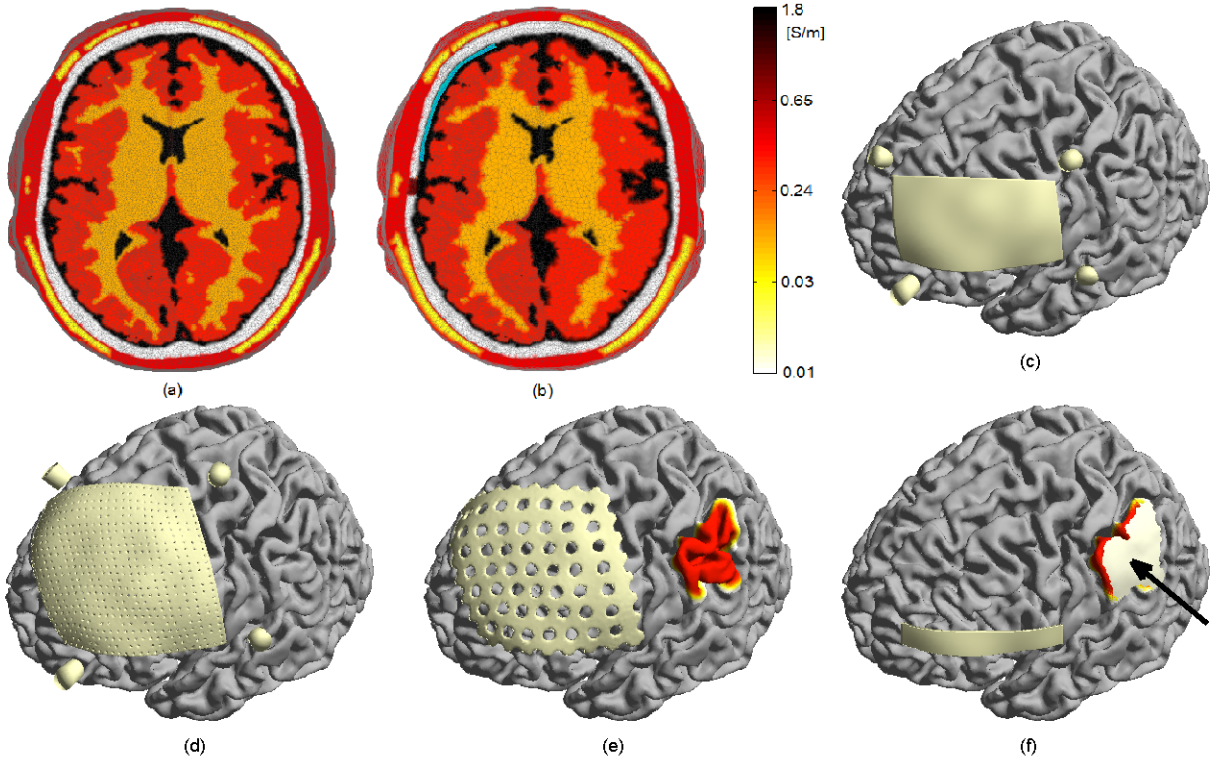

Figure 1: Head model used in the simulations. (a – b) Slice of the tessellated model showing the conductivity of the elements, in (b) the non-conducting subdural grid is shown in light blue. (c-f) Cortical surface model used in the simulations. The simulated subdural grids and skull holes are also shown. (c) 4 x 8 cm subdural grid and skull holes. (d) 8 x 8 cm subdural grid and skull holes. The grid model shown is fenestrated with many small holes (1 mm diameter). (e) 8 x 8 cm fenestrated subdural grid (6mm holes). (f) 1 x 8 subdural strip. In (e) and (f) a distributed generator is shown as an example. The arrow in (f) indicates the subdural surface patch in which the generator was projected to compute its subdural extent.

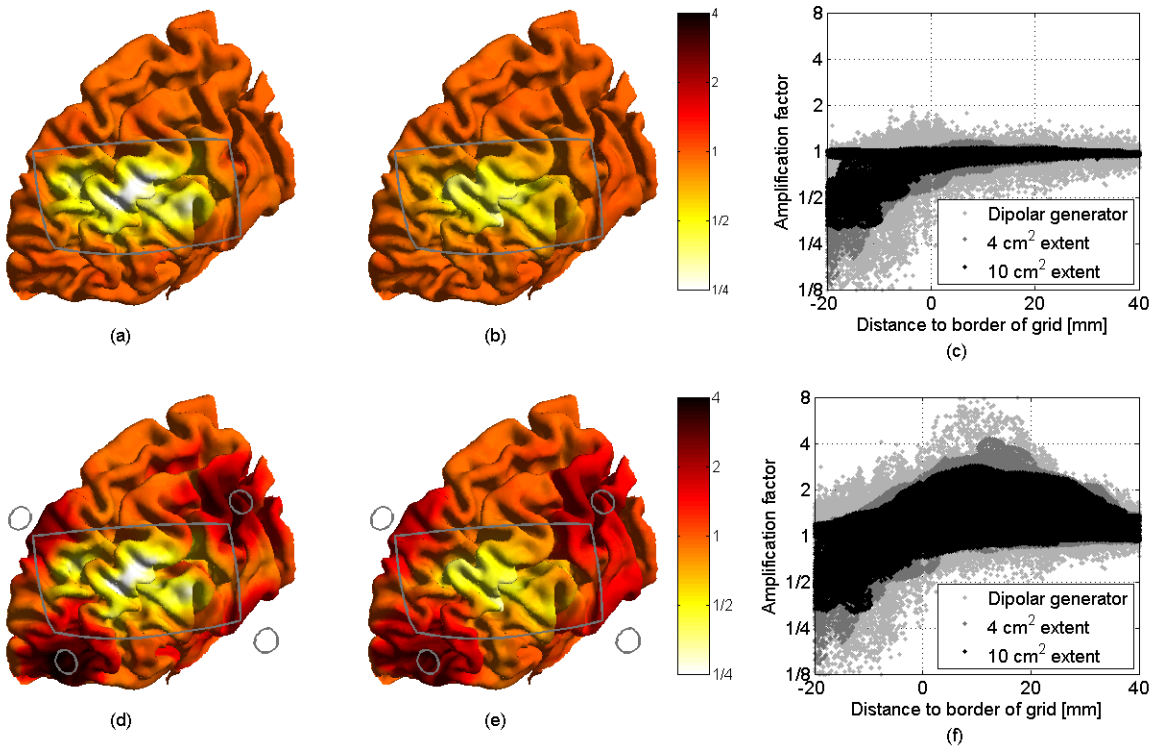

Figure 2: Amplification/attenuation factor of the subdural grid and skull holes for generators of different extents. The color of each point on the left frontal cortex indicates the amplification factor for a generator centered at that location. (a – b) Effect of the subdural grid. (d – e) Combined effect of the grid and skull holes. Generator extents: (a, d) Generators of 4 cm^2 subdural extent. (b, e) Generators of 10 cm^2 subdural extent. (c, f) Scatter plot of the amplification/attenuation factor versus distance to the border of the grid, for more than 58,000 generators on the left frontal lobe cortex. Negative distances correspond to generators under the grid, and positive distances to generators that are not directly under the grid. The amplification factor is shown for generators of three different extents (dipolar generators, 4 cm^2 and 10 cm^2). (c) Amplification/attenuation factor caused by the subdural grid. (f) Combined factor of the grid and skull holes.

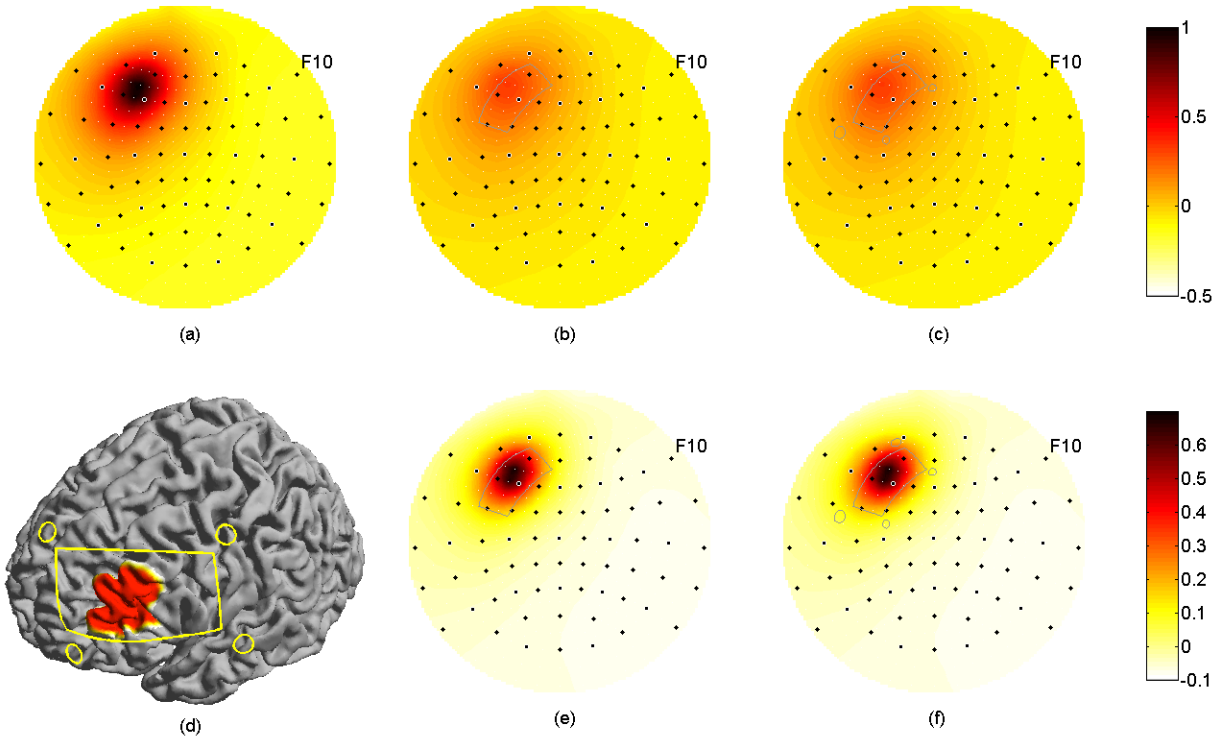

Figure 3: Example of the scalp potential of a generator under the subdural grid. (a) Normalized electric potential distribution on the scalp without the subdural grid, (b) with the grid, and (c) with the grid and skull holes. (a – c) are normalized by the same value, i.e. are in the same scale. (d) Location and extent of the generator in the cortical surface. The location of the grid and skull holes is shown schematically. (e – f) show the difference in the scalp electric potential distribution due to the presence of (e) the grid and (f) the grid and skull holes, compared to the scalp distribution when no grid is present. As the scale is normalized by the maximum scalp potential of the model without grid, (e) and (f) show that the largest difference in the scalp potential reaches 0.7 times this maximum value in the example, and the difference is largest over the center of the grid.

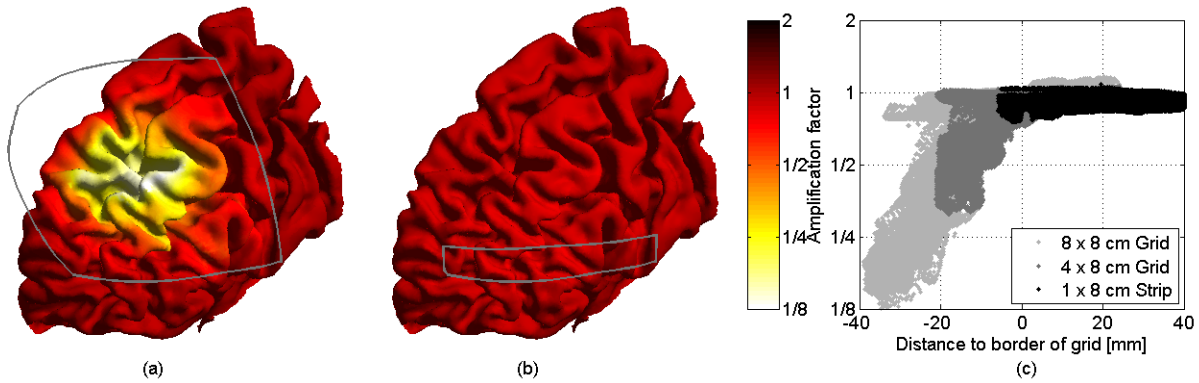

Figure 4: Amplification/attenuation factors for 10 cm^2 generators produced by subdural grids of different sizes. (a) An 8 x 8 cm subdural grid. (b) A 1 x 8 cm subdural strip. (c) Scatterplot comparing the amplification/attenuation factors as a function of the distance between the center of the generator and the border of the grid. Negative distances correspond to generators under the grid, and positive distances to generators that are not directly under the grid. The results from a 4 x 8 cm grid (Fig. 2b) are also included in the comparison.

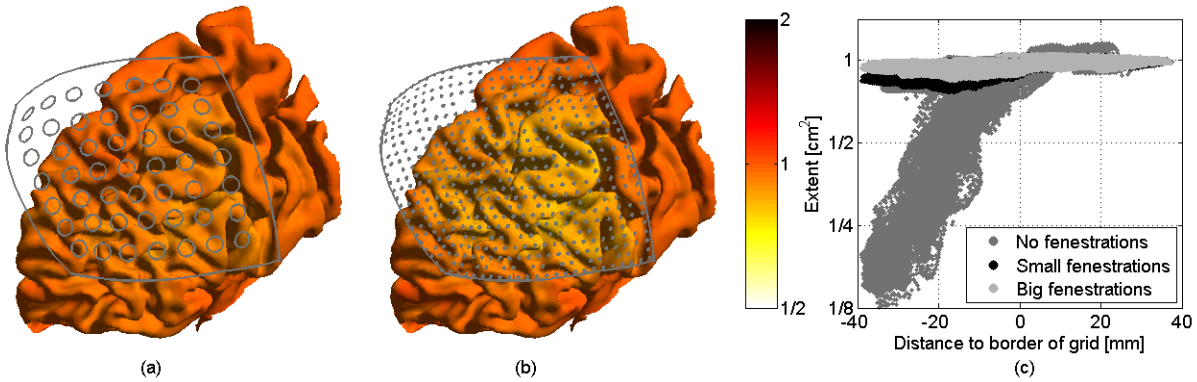

Figure 5: Amplification/attenuation factors for 10 cm^2 generators produced by 8 x 8 cm fenestrated grids. (a) A grid with large holes (6 mm diameter) (b) A grid with small holes (1 mm diameter). (c) Scatterplot comparing the amplification/attenuation factors as a function of the distance between the center of the generator and the border of the grid. Negative distances correspond to generators under the grid, and positive distances to generators that are not directly under the grid. The results from a grid without fenestrations (Fig. 4a) are also included in the comparison.

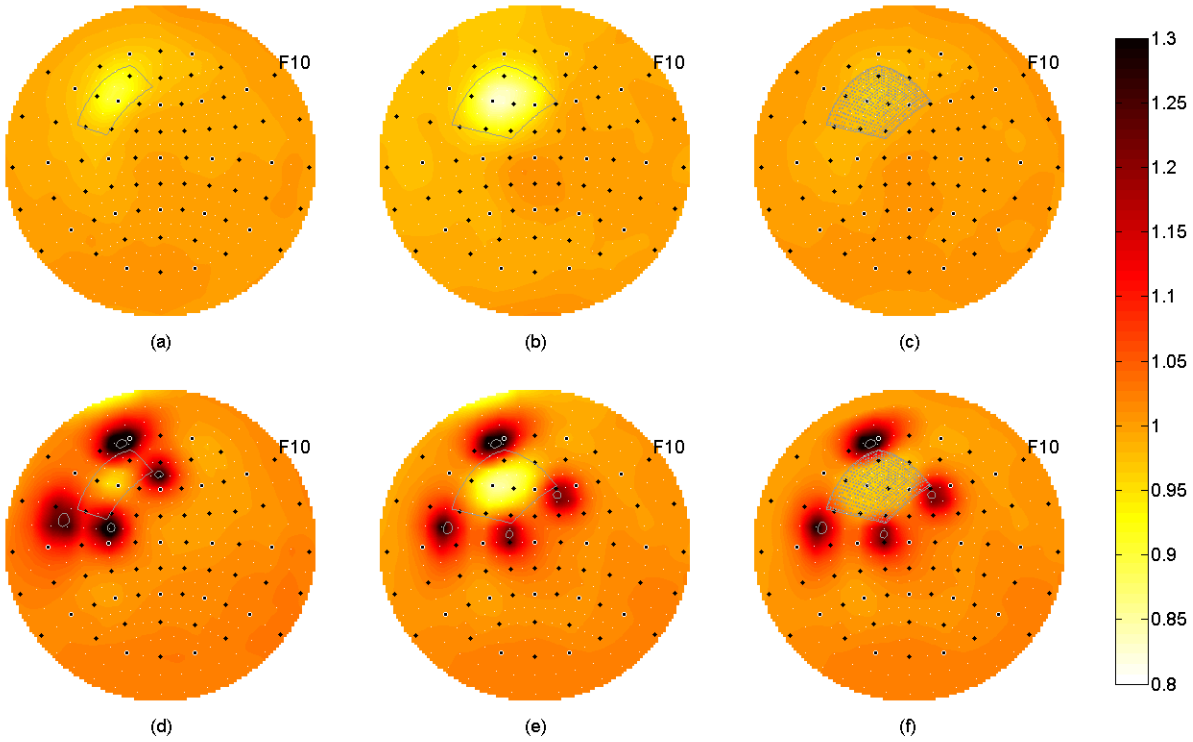

Figure 6: Effect of the subdural grid and skull holes on the scalp background brain activity level. Background level changes due to the presence of (a) a 4 x 8 cm subdural grid, (b) an 8 x 8 cm subdural grid, (c) the same 8 x 8 grid with small holes. (d-f) Idem when also including skull holes. In all cases the results are relative to the background level without subdural grid.

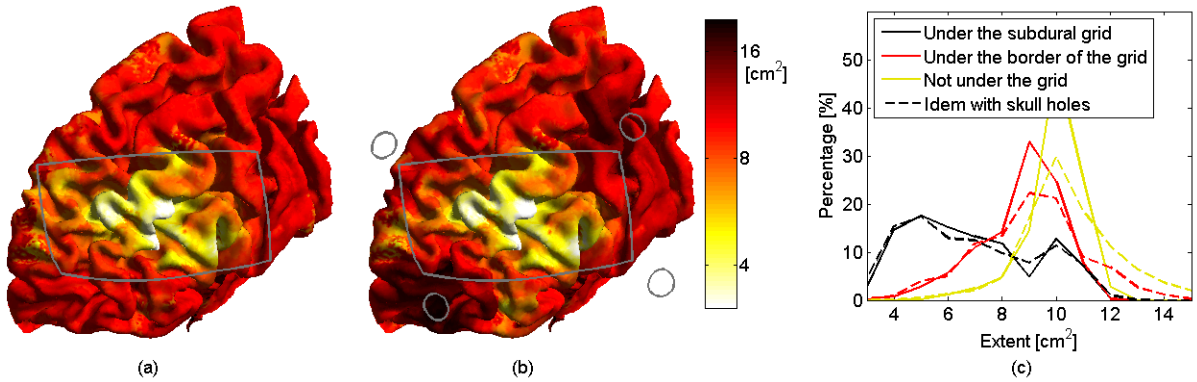

Figure 7: Effect of the 4 x 8 cm grid on the apparent extent of the generators. The color of each point of the left frontal lobe cortical surface indicates the extent of a generator centered at that point, which, when there is no grid, produces the same maximum signal to noise ratio on the scalp as a 10 cm^2 generator centered at the same point when the grid is present. (a) When only the grid is considered. (b) When the grid and skull holes are considered. (c) Same information presented differently: distribution of the extent of the generators, for generators with their center below the grid at a distance larger than 1 cm from the border, generators with their center under the grid but at a distance between 0 and 1 cm from the grid's border, and generators with their center not under the grid.

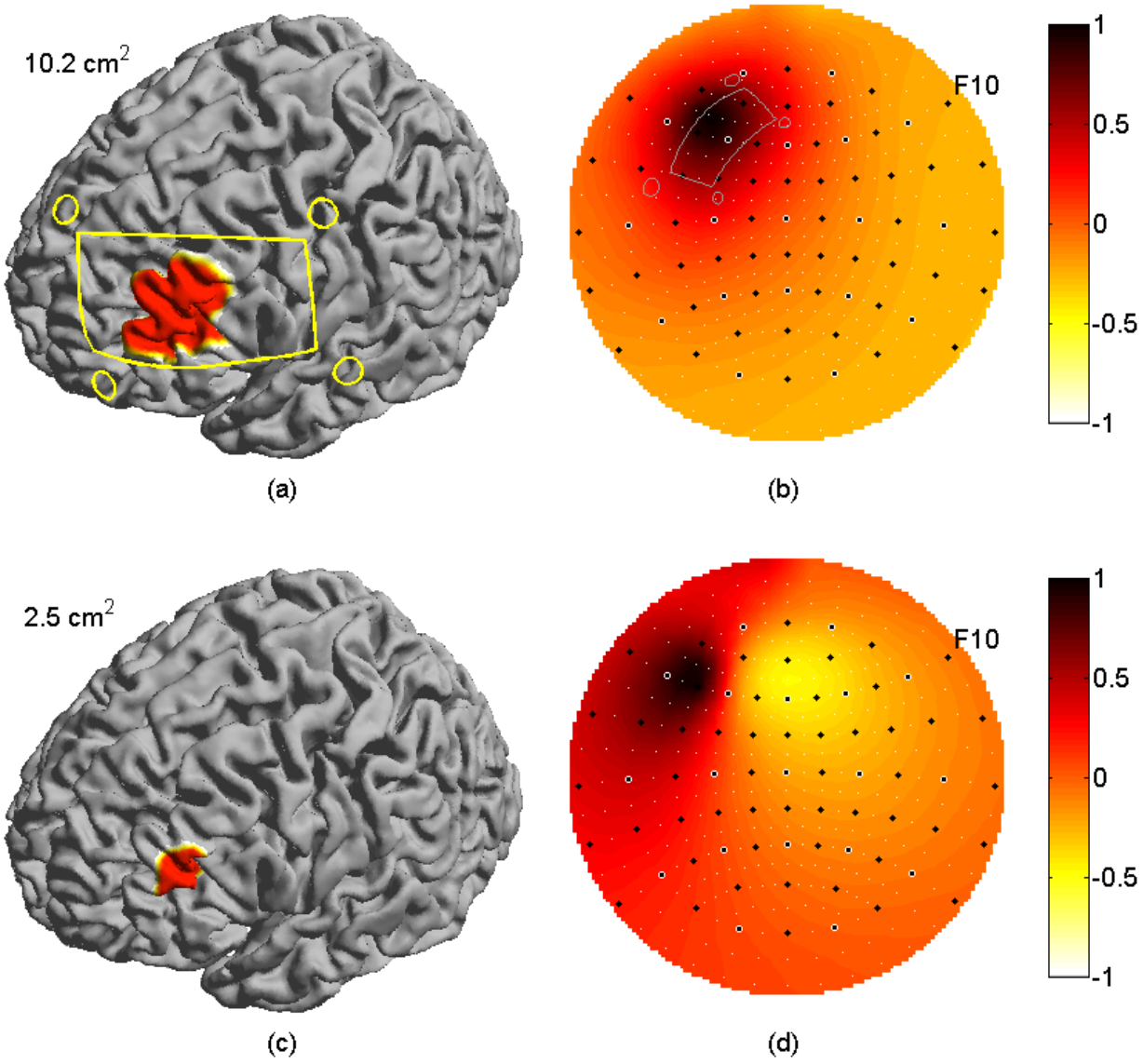

Figure 8: Example of a 2.5 cm^2 generator that produces the same maximum scalp potential as a 10 cm^2 generator centered at the same point but under a subdural grid. (a) Location and extent of the larger generator under the grid. (b) Scalp electric potential distribution of the generator under the grid. (c) Location and extent of the smaller generator, no grid. (d) Scalp electric potential distribution of the smaller generator. (b) and (d) are normalized by the same value, i.e. are in the same scale.

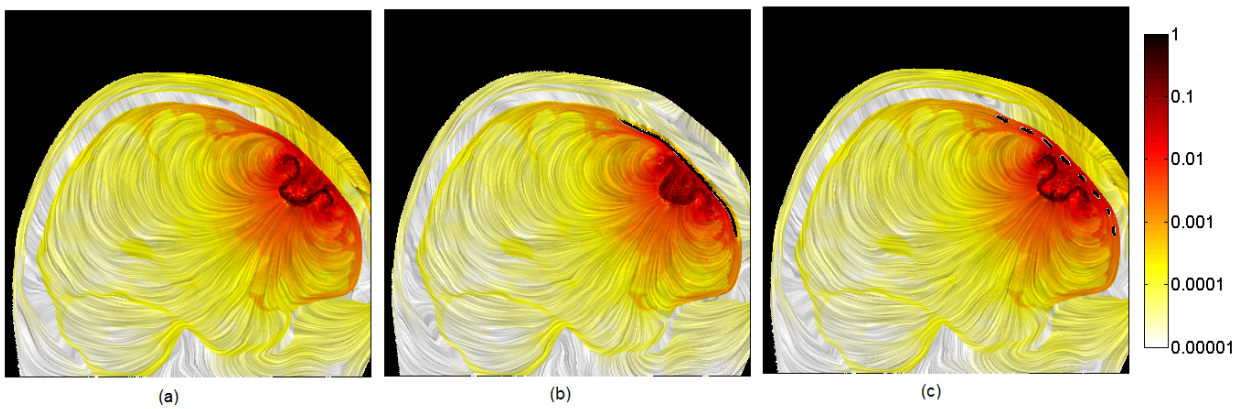

Figure 9: Normalized current density distribution on a head slice. (a) Without subdural grid. (b) With subdural grid. (c) With fenestrated grid.